Chapter 2

Comprehensive determination of protein tyrosine pK_a values using indirect ^{13}C NMR spectroscopy: an application to photoactive yellow protein

N. Alia Oktaviani*[1], Trijntje J. Pool*[1], Hironari Kamikubo[2], Jelle Slager[1], Ruud M. Scheek[1], Mikio Kataoka[2], Frans A.A. Mulder[1]

* these authors contributed equally to the work

[1]*Groningen Biomolecular Sciences and Biotechnology Institute, University of Groningen, Nijenborgh 7, 9747 AG Groningen, The Netherlands*

[2]*Graduate School of Materials Science, Nara Institute of Science and Technology, 8916-5 Takayama, Ikoma, Nara 630-0192, Japan*

Biophys J. 2012 Feb 8;102(3):579-86.

2.1 Abstract

Upon blue-light irradiation, the bacterium *Halorodospira halophila* is able to modulate the activity of its flagellar motor and thereby evade potentially harmful UV radiation. The 14 kDa soluble cytosolic photoactive yellow protein (PYP) is believed to be the primary mediator of this photophobic response, demonstrating a UV/Vis absorption spectrum that closely matches the bacterium's motility spectrum. In the electronic ground state the *p*-coumaric acid (*p*CA) chromophore of PYP is negatively charged and forms two short hydrogen bonds to the side chains of glutamic acid 46 and tyrosine 42. The resulting acid triad is central to the marked pH-dependence of the optical-absorption relaxation kinetics of PYP. Here, we demonstrate a NMR approach to sequence-specifically follow all tyrosine side chain protonation states in PYP from pH 3.41 to 11.24. The indirect observation of the non-protonated $^{13}C_{\gamma}$ resonances in sensitive and well-resolved two-dimensional ^{13}C-^{1}H spectra proved pivotal in this effort, as observation of other ring-system resonances was hampered by spectral congestion and line broadening due to ring flips. We observe three classes of tyrosine residues in PYP, which exhibit very different pK_a values, depending on whether the phenolic side chain is solvent exposed, buried or hydrogen bonded. In particular, our data show that tyrosine 42 remains fully protonated in the pH range 3.41 - 11.24 and that pH-induced changes observed in the photocycle kinetics of PYP cannot be caused by changes in the charge state of Y42. It is therefore very unlikely that the *p*CA chromophore undergoes changes in its electrostatic interactions in the electronic ground state.

2.2 Introduction

Photoactive yellow protein is a soluble, cytosolic protein from the purple phototropic eubacterium *Halorhodosphira halophila*. PYP shows a UV absorption spectrum that closely matches the wavelength dependence of the escape of the bacterium from potentially harmful blue-light radiation (Sprenger et al., 1993). Due to this observation PYP has become an important example of a soluble bacterial light sensor, and a rich model system for the study of PER-ARNT-SIM (PAS) domain signaling (Pellequer et al., 1998).

PYP consists of 125 residues which form a 6-stranded β-sheet flanked by 5 α-helices in an α/β fold (Borgstahl et al., 1995). In the active site, the *para*-coumaric acid (*p*CA) chromophore forms a thioester bond to the side chain of C69. This chromophore is stabilized by the formation of two short hydrogen bonds (SHBs) between *p*CA and E46, and also between *p*CA and Y42 (Anderson et al., 2004; Fisher et al., 2007), as shown in Fig 1.

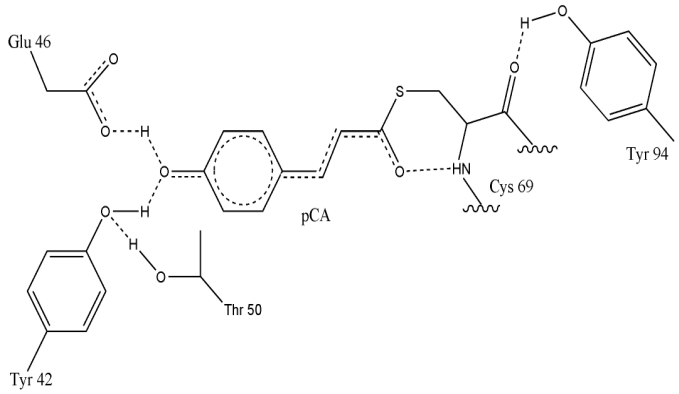

Figure 2.1. The hydrogen-bond network of PYP in the active centre.

Recent high-resolution neutron and X-ray crystallographic structures reveal a shared low-barrier hydrogen bond (LBHB) between *p*CA and E46, whereas the hydrogen bond between *p*CA and Y42 is qualified as a short ionic hydrogen bond (SIHB) (Yamaguchi et al., 2009) (6). The two hydrogen bonds have been detected using 1D ^{1}H NMR by Sigala *et al* (Sigala et al., 2009). As depicted in Fig 1, the phenolic oxygen of Y42 also participates as a proton acceptor in the hydrogen-bond formation with the hydroxyl proton of T50. Y94

is also involved in the hydrogen-bond network in the active centre by donating its side chain proton to the backbone oxygen of C69 (Anderson et al., 2004; Brudler et al., 2000).

Upon blue-light irradiation, PYP undergoes a number of changes in its optical properties that are associated with changes in its structure (Imamoto and Kataoka, 2007; Imamoto et al., 1997; Xie et al., 1996). Initially, the *para*-coumaric acid (*p*CA) chromophore undergoes a series of rapid bond isomerizations on the picosecond time scale to the pR state. This process is followed by proton transfer in the microsecond time scale, which involves the dissolution of the shared LBHB (Yamaguchi et al., 2009) and protonation of *p*CA to form the pB' state(Carroll et al., 2010; Ujj et al., 1998). Spectroscopic evidence has shown that the N-terminal domain of PYP dissociates from its PAS domain and becomes unfolded. This state is then recognized as pB, in which λ_{max} of the chromophore absorption changes from 446 nm (in the ground state, pG) to 355 nm (in the pB state) (Düx et al., 1998; van der Horst et al., 2001). Finally, the intermediate (pB) relaxes slowly (sub-second) to the initial pR state, a process associated with the formation of the central β sheet and part of the helical structures, and succeeded by a consolidation of structure around the *p*CA chromophore (Düx et al., 1998). The time scales indicated here are only approximate, and display a strong pH dependence (Brudler et al., 2000; Hendriks and Hellingwerf, 2009; Imamoto et al., 2004). Central to the mechanism of photoactivation is the presence of a low-barrier hydrogen bond (LBHB) between *p*CA and E46 in the ground state. Photoactivation causes a breaking of this LBHB, followed by significant conformational rearrangement of all helices except part of helix α_5 (Düx et al., 1998). Thus a distinct epitope is presented for interaction with downstream partners in the phototactic response, although the corresponding signaling pathway still remains unknown (Imamoto and Kataoka, 2007).

In order to study the role of electrostatic interactions in protein function, it is important to assemble a set of NMR experiments that can accurately determine the protonation states of titratable amino acid side chains. Individual pK_a's can be determined by following chemical shifts of nuclei in the amino acid side chain. The first, obvious choice is ^{1}H NMR (Karplus et al., 1973), because of its high NMR receptivity, so it does not require any

isotopic enrichment. However, there are several challenges: the ^{1}H NMR spectrum of larger proteins is highly crowded, the response of ^{1}H chemical shifts to protonation state is often relatively small, and ^{1}H chemical shifts are sensitive to other ionization equilibria than that of the amino acid to which the proton is attached (Karplus et al., 1973). The chemical shifts of ^{13}C or ^{15}N nuclei at the site of (de)protonation tend to undergo larger (> 1 ppm) chemical-shift changes, and are therefore ideal reporters of protonation states. Moreover, such large variations in nuclear shielding are caused mainly by changes in the electron distribution within the side chain, rather than by charges developing in the environment, and can therefore be used as more selective probes of protonation states and pK_a values of amino acid side chains.

To accurately determine the protonation states of tyrosine residues, one can use several ^{13}C chemical shifts as reporters for the charge state of the tyrosine ring (Table 1 and Figure 2) (Norton and Bradbury, 1974).

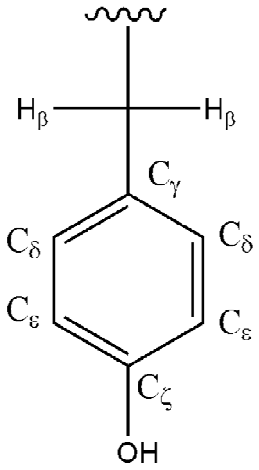

Figure 2.2 Tyrosine side chain.

Table 2.1. ^{13}C chemical shift reporters in the tyrosine side chain and their corresponding chemical shift changes upon deprotonation (Norton and Bradbury, 1974).

Carbon chemical shift reporter	Δδ (ppm)
Cγ	-6.2
Cδ	0
Cε	+3.3
Cζ	+10.4

1D ^{13}C NMR on uniformly ^{13}C-enriched protein samples is hindered by the presence of ^{13}C-^{13}C splittings in the spectrum and additional overlap with the $^{13}C_z$ signals of arginines. Therefore, 1D ^{13}C NMR has been combined with selective incorporation of ^{13}C-Tyr(Kato-Toma et al., 2003; Ugurbil and Bersohn, 1977; Wilbur and Allerhand, 1976). In this approach, the assignments were obtained by removing individual tyrosine residues through

mutagenesis, requiring the parallel production and purification of multiple protein samples. It is furthermore required that the removal of each tyrosine does not significantly perturb the structure, so that the spectral change can be unambiguously attributed to the mutation site.

Alternatively, 2D ^{1}H-^{13}C or ^{1}H-^{15}N NMR experiments applied to uniformly $^{13}C/^{15}N$ enriched proteins are ideally suited to record the heteronuclear chemical shifts as a function of pH, as they offer excellent sensitivity and resolution, and permit the comprehensive and residue-specific assignments of individual amino acid resonances. So far, experiments of this type have been described for Asp, Glu, Lys, Arg and His side chains, as well as the C- and N-termini(André et al., 2007; Hass et al., 2009; Oda et al., 1994), but an analogous method for addressing Tyr charge states was missing until recently (Baturin et al., 2011).

In this study, we present a strategy for the comprehensive determination of pK_a values of the protein. We investigate the pH-dependent protonation state of Y42, which forms a short hydrogen bond to the *p*CA chromophore, stabilizing its delocalized negative charge. The presence of a short hydrogen bond under physiological condition has been firmly established on the basis of X-ray and neutron crystallographic structures (Yamaguchi et al., 2009), NMR spectroscopic observation (Düx et al., 1998; Sigala et al., 2009), as well as other spectroscopic data and theoretical calculations (Boggio-Pasqua et al., 2009). However, the basis for the pH dependence of the photocycle kinetics is not fully understood at atomic resolution. We shall show that Y42 remains fully protonated in the pH range 3.41 -11.24 indicating that the pH dependence of the PYP photocycle kinetics cannot be caused by changes in the charge state of Y42, and it is therefore very unlikely that the *p*CA chromophore undergoes changes in its electrostatic interactions in the electronic ground state.

2.3 Material and Methods

2.3.1 Sample preparation

Uniformly ^{13}C, ^{15}N labeled wild type PYP was produced in M9 minimal medium

containing uniformly ^{13}C-enriched glucose and $^{15}NH_4Cl$ and purified as described previously (Mihara et al., 1997). NMR samples contained ~1.0 mM of doubly labeled [^{13}C, ^{15}N] PYP, 0.15 mM DSS, 10% D_2O and either 15 mM sodium acetate $-d_3$, 5 mM potassium phosphate or 15 mM sodium bicarbonate as buffer for the pH ranges pH 3.4 - 5.8, 5.9-8.6, 8.7-11.24, respectively. The pH was changed in steps of 0.2 pH units by adding a few μL of concentrated HCl or NaOH solution. For calibrating the pH meter (PB-11-P11, Sartorius mechatronics), standard calibration buffers of pH 4.0, 7.0 and 10.0 were used. For measurements below pH 4 and above pH 10, a 0.1 M HCl solution (pH 1.0) and a 10 mM NaOH solution (pH 12) were used for calibration.

2.3.2 NMR spectroscopy

All NMR experiments were carried out using a Varian Unity INOVA 600 MHz spectrometer equipped with a pulsed field-gradient probe at 293 K. All aromatic proton-carbon correlations were established from 2D constant-time ^{1}H-^{13}C HSQC spectra. This experiment was performed with the carrier position at 125 ppm in the ^{13}C domain. 512 (H^{aro}) x 128 (C^{aro}) complex points were recorded, with maximum acquisition times of 64 and 16 ms for ^{1}H and ^{13}C, respectively. An inter-scan delay of 1 second was used with 2 scans per FID, giving rise to a measurement time of 9 minutes.

To obtain the signal from 2-bond correlations between C_ζ and H_ε, a constant-time ^{1}H-^{13}C HSQC experiment was performed with the INEPT delay set to 24 ms (Takeda et al., 2009). 512 (H^{aro}) x 128 (C^{aro}) complex points were recorded, with maximum acquisition times of 64 and 16 ms for ^{1}H and ^{13}C, respectively. The number of scans per FID was 96, and the inter-scan was 1 s. The total experiment time was 7.5 hours.Cγ-Hβ correlations in tyrosine side chains were recorded using a 2D CG(CB)HB experiment with constant-time C_γ evolution (Prompers et al., 1998). The spectra were acquired using 90 (C_γ) x 512 (H_β) complex points with maximum evolution times equal to 15 and 64 ms, respectively. The carrier position was placed at 130 ppm in the ^{13}C domain to excite the C_γ region. An interscan delay of 1 s was used and 20 scans per FID were recorded, giving a total experiment time of about 1 hour for every 2D spectrum.

All spectra were processed using NMRPipe (Delaglio et al., 1995) and analysed using SPARKY (Goddard and Kneller, 2003). Mirror-image linear prediction was applied during processing to extend the ^{13}C time-domain signal and improve the spectral resolution. All chemical shifts were referenced to DSS based on IUPAC recommendation (Markley et al., 1998). All tyrosine peaks were assigned based on the strategy described by Oktaviani *et al* (Oktaviani et al., 2011). Complete assignment of PYP will be presented in a forthcoming publication.

2.3.3. Data analysis

The titration data for all tyrosine chemical shifts were fitted to the Henderson-Hasselbalch equation, appropriate for rapid exchange of the nuclei between the environments associated with the neutral and charged states of the side chain:

$$\delta_{\mathrm{obs}} = \delta_{\mathrm{AH}} + \Delta\delta \frac{10^{n_H(\mathrm{pH}-\mathrm{pK_a})}}{1+10^{n_H(\mathrm{pH}-\mathrm{pK_a})}} \quad (1)$$

where δ_{AH} denotes the chemical shift for the protonated form, and $\Delta\delta = \delta_{A^-} - \delta_{AH}$ is the change in chemical shift upon *de*protonation. n_H is the Hill coefficient ($n_H > 1$ indicates apparent positive cooperativity). All calculations were performed using Mathematica (Wolfram Inc.).

2.4 Results and Discussion

As the chemical-shift response to (de)protonation is sufficiently large for $^{13}C\varepsilon$, the unambiguous determination of the charge state of individual tyrosine side chains could, in principle, be achieved by recording 2D HSQC or HMQC spectra, which exhibit high sensitivity. The 2D ^{1}H-^{13}C HSQC spectrum for PYP is shown in Figure 2. 3.

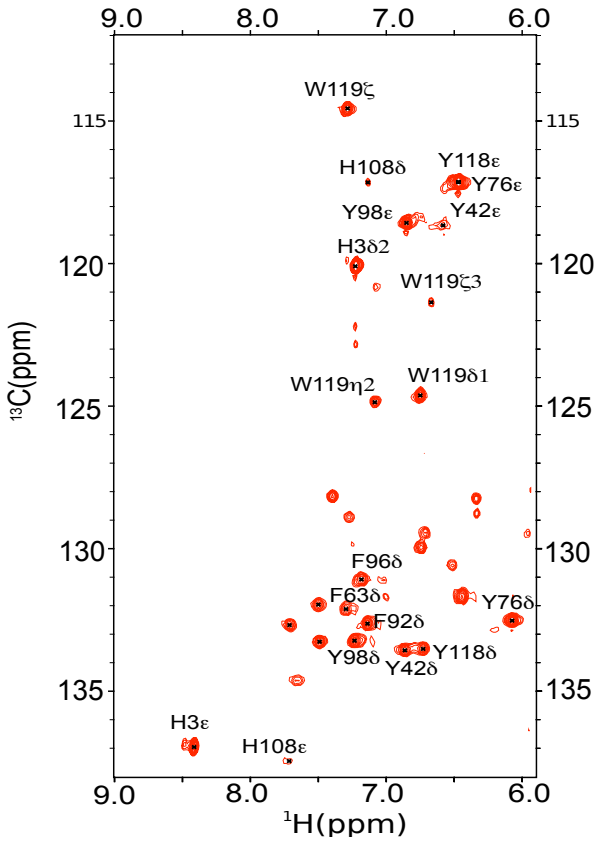

Figure 2.3. Region of the 2D aromatic ^{13}C-^{1}H HSQC spectrum for PYP containing the Tyr C-H correlations. Peak of Y118 Cε overlaps with Y76 Cε. Signals for Trp, and His side chains also fall in this spectral region. Assignments of the correlations are indicated.

Signals for the surface-exposed residue Y98 are easily identified, Y76 overlaps with Y118, but resonances for Y42, Y94 are weak or invisible. This is probably due to the slow rotation of several tyrosines in the protein interior leading to exchange broadening. This may be a serious limitation for experiments that aim at utilising the Hd or He ring-proton resonances for other proteins as well.

Alternatively, 2D experiments that correlate ^{13}C with a ^{1}H nucleus two bonds removed via successive homonuclear and heteronuclear transfer through large one-bond couplings have been designed for the determination of acidic side chain groups of Asp and Glu and the C-terminus (Oda et al., 1994). These experiments offer excellent sensitivity and resolution. In

a recent paper, (Baturin et al., 2011) a 2D HE(CE)CZ pulse sequence, which correlates H_ε and C_ζ, was successfully applied to the tyrosine pK_a determination in *Bacillus circulans* Xylanase. An approach to assign Tyr $^{13}C_\zeta$ in the context of SAIL isotope labeling (Takeda et al., 2009) employs the two-bond H_ε-C_ζ coupling. This experiment is also applicable to uniformly enriched samples, where three bond Hδ-Cγ correlations may be observed in addition. Unfortunately, these experiments suffer from sensitivity losses in the case of ring flips, when the Hδ and Hε protons move between different magnetic environments. In the case of PYP, only signals from Y76 and Y98 are observed using the latter experiment, as shown in Figure 2. 4.

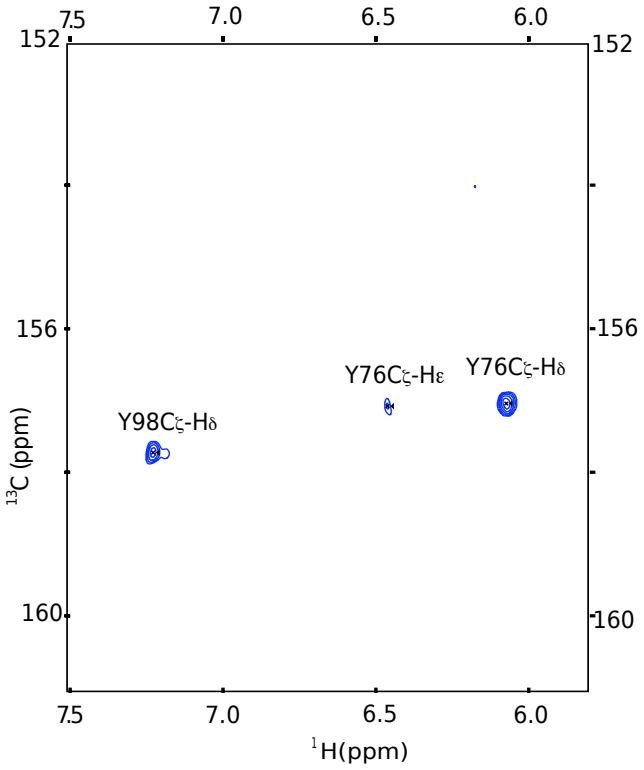

Figure 2. 4. 2D ^{13}C-^{1}H HSQC spectrum that correlates Hδ and Hε with Cζ for Tyr residues of PYP. Assignments of the correlations are indicated. Signals for Y42, Y94, and Y118 were not observed.

A final alternative would be the indirect detection of the $^{13}C\gamma$ chemical shifts. These can be correlated to H_b chemical shifts via successive magnetization transfers through the large CγCβ ($^1J_{CC}$ ~ 45 Hz) and CβHβ ($^1J_{CH}$ ~ 130 Hz) coupling constants. This could be done via

an out-and-back HB(CB)CG experiment, but for larger proteins increased sensitivity can be obtained by avoiding one of the long and lossy homonuclear ^{13}C-magnetization transfer steps, by starting on the non-protonated $^{13}C_\gamma$((30) CG(CB)HB spectra are generally well resolved, even for larger proteins (> 20 kDa), as they exhibit significant variation in the Cγ chemical shift as a function of amino acid type and secondary structure, and because there are two non-equivalent protons available to read out the Cγ shift in the resulting 2D spectrum. Partial deuteration will improve the sensitivity of the technique for proteins with higher molecular weights (Gardner and Kay, 1998). Improved sensitivity of HB(CB)CG-type measurements have been reported with a ~50% level of deuteration (Prompers et al., 1998). For PYP, all tyrosine side chain signals were observable with good sensitivity, and there is not a single instance of overlap in the spectrum. In addition, we could detect the C_γ resonance of His3 (which showed a pK_a value of 6.5) but not that of His118. We note that His Cγ detection could be improved by ^{15}N decoupling during Cγ evolution, which was not done here.

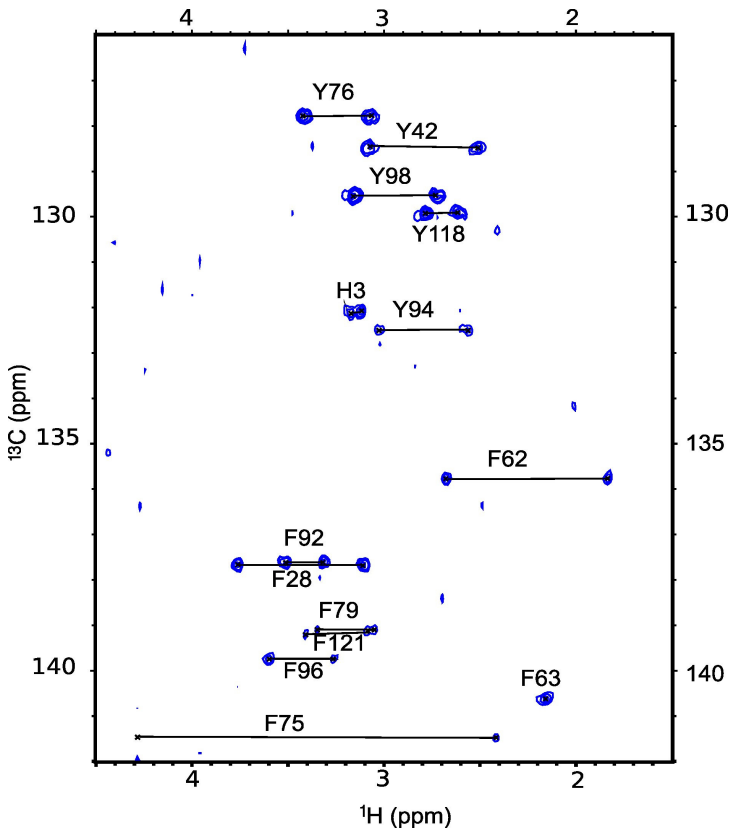

Figure 2.5. 2D CG(CB)HB spectrum that correlates $H_{\beta 2}/H_{\beta 3}$ with C_{γ} for Tyr residues of PYP. His correlations were also detected. Assignments are indicated.

We followed the various chemical shifts that can be used as reporters of the side chain charge state for the two tyrosine residues that titrate below pH 11. These are given in Table 2. For Y76 and Y98 it can be confirmed that the chemical shifts of Cγ and Cε stand out as responsive reporters for the side chain protonation state, and that the Cδ resonance positions cannot be employed for this purpose. The small pH-dependent changes measured for the ring-proton chemical shifts yield pK_a values that are within 0.1 from those determined by ^{13}C chemical shifts. However, small changes in ^{1}H shifts can also result from changes in the charge states of nearby side chains. In particular, the pK_a values of Lys amino groups are very similar to those of Tyr side chains, and this could lead to misinterpretation. The fact that this does not seem to occur for PYP is due to the spatial separation of the titrating groups. The fact that ^{1}H chemical shifts are particularly reactive

to changes in the local distribution of charges has been documented in the literature (Harris and Turner, 2002).

Table 2.2 Best-fit values for the pH-dependent ^{13}C chemical-shift changes and pK_a's of Y76 and Y98 of PYP.

residue	Nucleus[a]	δ_0 (ppm)	$\Delta\delta$ (ppm)	pK_a	n_H
Y76	Cδ	132.47	-	-	-
	Cε	117.1 ± 0.1	2.23 ± 0.04	10.14 ± 0.02	1.24 ± 0.06
	Cγ	127.8 ± 0.1	-3.77 ± 0.08	10.21 ± 0.02	1.16 ± 0.04
	(at $H\beta_{2/3}$)				
	Hβ	3.003	-	-	-
	Hδ	6.05	-	-	-
	Hε	6.46 ±0.04	0.162±0.004	10.1 ±0.03	1.3± 0.1
global fit[b]	Cδ	132.47 ± 0.02	-0.08 ± 0.02		
	Cε		2.30 ± 0.04	10.20 ± 0.03	1.18 ± 0.06
	Cγ	117.1 ± 0.1	-3.73 ± 0.06		
		127.7 ± 0.1			

residue	Nucleus[a]	δ_0 (ppm)	$\Delta\delta$ (ppm)	pK_a	n_H
Y98	Cδ	133.00	-	-	-
	Cε	118.6 ± 0.1	2.8 ± 0.1	10.32 ± 0.03	1.12 ± 0.08
	Cγ	129.5 ± 0.1	-4.8 ± 0.1	10.20 ± 0.01	1.54 ± 0.06
	(atHβ2/3)				
	Hβ	3.15	-	-	-
	Hδ	7.231±0.004	0.157±0.04	10.43±0.03	1.05±0.05
	Hε	6.85± 0.01	0.28± 0.01	10.37±0.04	1.14±0.1
global fit[b]	Cδ	133.00 ± 0.02	-0.23 ± 0.02	10.21 ± 0.03	1.48 ± 0.08

Cε	118.6 ± 0.1	2.5 ± 0.1
Cγ	129.5 ± 0.1	-4.8 ± 0.1

[a] Cδ, Cε, Hδ and Hε resonances were monitored by ^{13}C-^{1}H HSQC spectroscopy; Cγ and Hβ resonances were recorded by CG(CB)HB spectroscopy.

[b] for global fitting the four titrations pertaining to the same tyrosine ring (probed at CγHβ2, CγHβ3, CδHδ and CεHε) were combined and fitted simultaneously to a model with one pK_a and one n_H for that tyrosine. Standard deviations for the best-fit parameters resulting from the individual fits were estimated by analysis of the c^2 function (Berendsen, 2011); for the global-fit parameters the standard deviations were estimated using a Monte Carlo protocol in which estimated standard deviations per data point (0.05 in pH and 0.03 ppm in chemical shift) were used. See text for a further discussion of the accuracy of these results.

Figure 2.6.A shows the location of the two solvent-exposed Tyr residues in PYP, together with titration curves of their $^{13}C\gamma$ resonances. The pK_a's for the solvent exposed residues Y76 and Y98 are 10.20 and 10.21, respectively, which is 0.5 units above the intrinsic pK_a reported for Tyr in aqueous solution (Harris and Turner, 2002). Since the net protein charge is about -6 at pH 9, this upshift of 0.5 units (which corresponds to an energy difference of about 2.8 kJ/mol) is probably due to coulombic forces that favor the neutral form of Tyr.

Fits of Equation 1 to the experimental data improved significantly when the Hill parameters were allowed to become greater than 1, especially for Y98. This is unusual for pH titrations in compactly folded proteins, where electrostatic interactions between nearby groups that titrate in the same pH range are expected to lead to an apparent negative cooperativity (n_H<1). Even more puzzling is the observation that two titrations pertaining to the same residue (e.g. Y98, see Table 2) yield different values for the Hill parameter. We conclude that small systematic errors (e.g. in the measurements of the highest pH values) must be part of the explanation. However, we also note that structural rearrangements in the direct environment of Tyr residues (in response to the increasing

density of negative charges) can in principle explain apparent positive cooperativity in their titration curves.

The fact that the $^{13}C\delta$ resonance shifts 0.23 ppm downfield in the pH range around 10.5 (Table 2) is another indication that structural rearrangements must occur, since the $^{13}C_\delta$ chemical shift is normally unresponsive to ionization of the side chain (Norton and Bradbury, 1974).

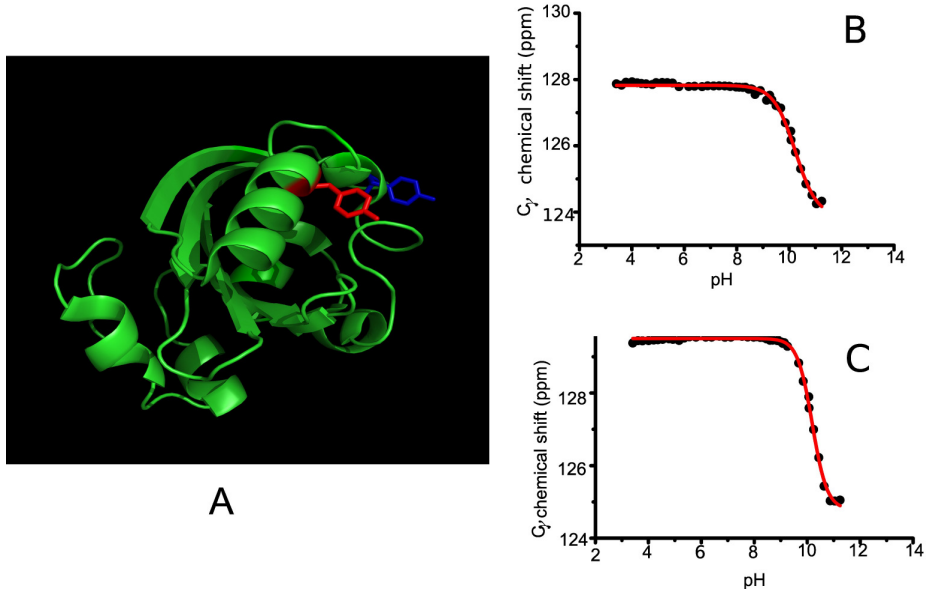

Figure 2.6. (A) PYP structure with the solvent-exposed residues Y76 (red) and Y98 (blue) indicated. pH titration profile of Y76 (B) and Y98 (C) using the $^{13}C\gamma$ chemical shifts as reporters.

As shown in Figure 2.7(A), Y118 is partly (9%) buried within the protein interior but its hydroxyl group is not involved in hydrogen bonding. The titration curve for the $^{13}C\gamma$ of Y118 is shown in Fig 7B. At the highest pH value the $^{13}C\gamma$ resonance has moved only -0.7 ppm. Assuming that $\Delta\delta$= -4 ppm (similar to the value measured for Y76), its estimated pK_a based on Eq 1 is 11.6, which is higher than those of the solvent-exposed residues Y76 and Y98. Substitution of $\Delta\delta$ values within the range -3 to -6 ppm, yielded estimated pK_a values between 11.4 and 12.0. The difference in the pK_a value of 1.4 pH unit between

solvent-exposed tyrosine and buried tyrosine can be explained by the different dielectric properties of water as a solvent and the protein interior which is more hydrophobic. The more polar the environment, the more easily an acid/base can be ionized. Thus, in the hydrophobic environment of Y118, its pK_a has shifted to a higher value.

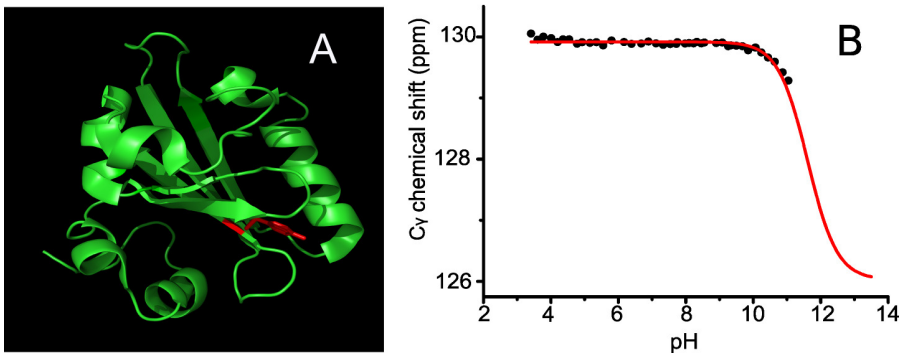

Figure 2. 7. Buried Y118 in PYP structure (A) and its corresponding pH titration profile using the ^{13}Cγ chemical shift as reporter (B).

The two remaining tyrosine residues in PYP, Y42 and Y94 are 82% and 27% buried, respectively, and involved in hydrogen bonding. Their location in the protein is indicated in Fig 2.8A. As the changes in their $^{13}C_\gamma$ chemical shifts are less than 0.1 ppm up to pH 11.24, the pK_a values of those side chains are significantly higher than 13, and cannot be determined reliably. The pK_a value of Y42 is of special mechanistic interest in the case of PYP, as this side chain shares a proton with the *p*CA chromophore, and forms a short hydrogen bond. Our data demonstrate that this hydrogen bond is extremely stable and remains intact over the entire pH range, from 3.41 to 11.24 (see Figure 2.8 (B), black). In this pH range, the protein is folded and the active centre is intact. However, the disruption of the hydrogen-bonding network involving the chromophore at very low pH (<3) results in partial protein unfolding (Craven et al., 2000), whereas at very high pH (>11) it leads to hydrolysis of the thioester bond that connects the *p*CA chromophore to C69 (Hoff et al., 1996). Y42 is also known to play an important role in stabilizing the native conformation of the *p*CA chromophore through hydrogen bonding. The mutation of Y42 into Phe (Y42F) disrupts the hydrogen-bond network between Y42 and the *p*CA chromophore as well as that between Y42 and the hydroxyl group of T50. This causes the distance between

Y42and T50 to increase due to van der Waals repulsion, and movement of the *p*CA chromophore toward T50. As a consequence, a second conformation of the *p*CA chromophore can be observed in the protein population as a shoulder in the UV/Vis spectrum at 391 nm (Brudler et al., 2000). However, the Y42F mutation does not have a significant effect on the pH dependence of the photocycle kinetics. The maximum rate constant for the transition of pR to pB in the Y42F mutant occurs at a similar pH, compared to wild-type PYP(Brudler et al., 2000). This finding agrees with our result that Y42 remains fully protonated in the pH range 3.41-11.24, which makes it unlikely that pH-induced changes observed in the photocycle kinetics of PYP are caused by changes in the electrostatic interactions involving the chromophore in the ground state.

Y94 is also buried and donates a hydrogen bond to the backbone of C69 and the hydroxyl side chain of serine 72 (S72). Fig 2.8 (B) (blue) shows that the protonation state of Y94 is pH-independent, indicating that Y94 is protonated over the entire pH range 3.41-11.24. Although there is no direct hydrogen bond between Y94 and the *p*CA chromophore, the stability of the hydrogen-bond network over a wide pH range may be important also for the stability of the thioester bond between C69 and *p*CA.This result is supported by the fact that the mutation Y94A shifts the absorption maximum by 4 nm towards the blue (442 nm) (Morishita et al., 2007). In agreement with these findings spectroscopic studies also imply that the hydrogen bond between the side chain of Y94 and the hydroxyl side chain of S72 is important for maintaining the helical secondary structure (Morishita et al., 2007).

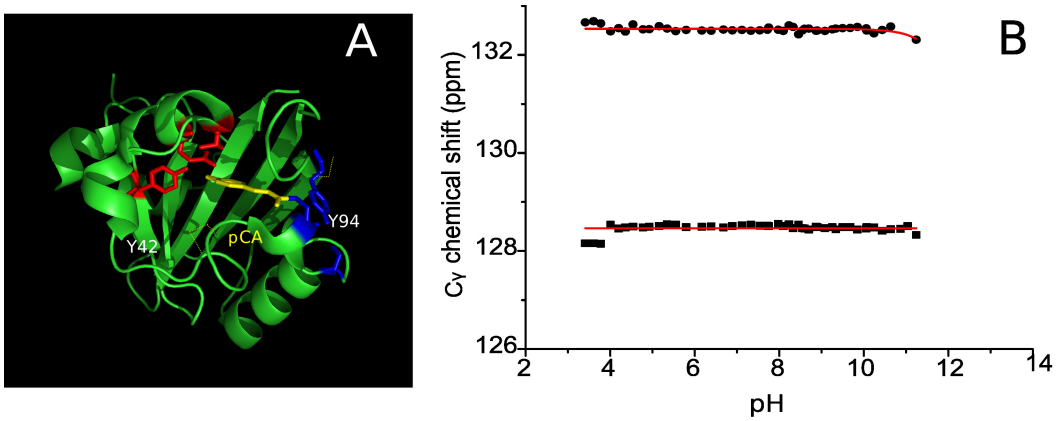

Figure 2.8. Hydrogen-bonded Tyr side chains in PYP. Y42 forms a hydrogen bond to *p*CA and the hydroxyl group of T50, whereas Y94 forms hydrogen bonds to the backbone of C69 and the hydroxyl group of S72 (A). pH titration profile of Y42 (below) and Y94 (above) using the $^{13}C_\gamma$ chemical shift as reporter (B).

2.5 Conclusions

We present an NMR approach based on 2D C_γ-H_β correlation spectroscopy to determine the residue-specific pK_a values of individual Tyr side chains in native proteins with high sensitivity and resolution. This approach offers a number of advantages over existing practices. Our approach does not require mutagenesis to assign the NMR resonances and facilitates the complete and comprehensive analysis of electrostatic interactions involving tyrosine side chains in proteins.

For photoactive yellow protein from *H. halophila*, we were able to determine the pH-dependence of the protonation states of all individual Tyr side chains. In PYP we observe three classes of tyrosines based on their titration behavior: solvent exposed (Y76 and Y98), buried in the hydrophobic environment (Y118) and hydrogen bonded (Y42 and Y94), with pK_a values of ~10, 12 and above 13, respectively. Our study also shows that the short hydrogen bonds to the *p*-coumaric acid chromophore persist over the entire pH range where the protein is chemically and thermodynamically stable. Our data indicate that previous observations of pH-dependent changes in PYP photocycle kinetics cannot be caused by changes in the charge state of Y42, and it is therefore very unlikely that the *p*CA

chromophore undergoes changes in its electrostatic interactions in the electronic ground state.

2.6 Acknowledgements

This work was supported by a VIDI grant to F.A.A.M from the Netherlands Organization for Scientific Research (NWO).

2.7 References

Anderson, S., Crosson, S., and Moffat, K. (2004). Short hydrogen bonds in photoactive yellow protein. Acta Crystallogr. D Biol. Crystallogr. *60*, 1008–1016.

André, I., Linse, S., and Mulder, F.A.A. (2007). Residue-specific pKa determination of lysine and arginine side chains by indirect 15N and 13C NMR spectroscopy: application to apo calmodulin. J. Am. Chem. Soc. *129*, 15805–15813.

Baturin, S.J., Okon, M., and McIntosh, L.P. (2011). Structure, dynamics, and ionization equilibria of the tyrosine residues in Bacillus circulans xylanase. J. Biomol. NMR *51*, 379–394.

Berendsen, H.J.C. (2011). A student's guide to data and error analysis (Cambridge; New York: Cambridge University Press).

Boggio-Pasqua, M., Robb, M.A., and Groenhof, G. (2009). Hydrogen bonding controls excited-state decay of the photoactive yellow protein chromophore. J. Am. Chem. Soc. *131*, 13580–13581.

Borgstahl, G.E., Williams, D.R., and Getzoff, E.D. (1995). 1.4 A structure of photoactive yellow protein, a cytosolic photoreceptor: unusual fold, active site, and chromophore. Biochemistry *34*, 6278–6287.

Brudler, R., Meyer, T.E., Genick, U.K., Devanathan, S., Woo, T.T., Millar, D.P., Gerwert, K., Cusanovich, M.A., Tollin, G., and Getzoff, E.D. (2000). Coupling of hydrogen bonding to chromophore conformation and function in photoactive yellow protein. Biochemistry *39*, 13478–13486.

Carroll, E.C., Song, S.-H., Kumauchi, M., van Stokkum, I.H.M., Jailaubekov, A., Hoff, W.D., and Larsen, D.S. (2010). Subpicosecond Excited-State Proton Transfer Preceding Isomerization During the Photorecovery of Photoactive Yellow Protein. J. Phys. Chem. Lett. *1*, 2793–2799.

Craven, C.J., Derix, N.M., Hendriks, J., Boelens, R., Hellingwerf, K.J., and Kaptein, R. (2000). Probing the nature of the blue-shifted intermediate of photoactive yellow protein in

solution by NMR: hydrogen-deuterium exchange data and pH studies. Biochemistry *39*, 14392–14399.

Delaglio, F., Grzesiek, S., Vuister, G.W., Zhu, G., Pfeifer, J., and Bax, A. (1995). NMRPipe: a multidimensional spectral processing system based on UNIX pipes. J. Biomol. NMR *6*, 277–293.

Düx, P., Rubinstenn, G., Vuister, G.W., Boelens, R., Mulder, F.A., Hård, K., Hoff, W.D., Kroon, A.R., Crielaard, W., Hellingwerf, K.J., et al. (1998). Solution structure and backbone dynamics of the photoactive yellow protein. Biochemistry (Mosc.) *37*, 12689–12699.

Fisher, S.Z., Anderson, S., Henning, R., Moffat, K., Langan, P., Thiyagarajan, P., and Schultz, A.J. (2007). Neutron and X-ray structural studies of short hydrogen bonds in photoactive yellow protein (PYP). Acta Crystallogr. D Biol. Crystallogr. *63*, 1178–1184.

Gardner, K.H., and Kay, L.E. (1998). The use of 2H, 13C, 15N multidimensional NMR to study the structure and dynamics of proteins. Annu. Rev. Biophys. Biomol. Struct. *27*, 357–406.

Goddard, T.., and Kneller, D.. (2003). SPARKY 3 (San Fransisco: University California).

Harris, T.K., and Turner, G.J. (2002). Structural basis of perturbed pKa values of catalytic groups in enzyme active sites. IUBMB Life *53*, 85–98.

Hass, M.A.S., Yilmaz, A., Christensen, H.E.M., and Led, J.J. (2009). Histidine side-chain dynamics and protonation monitored by 13C CPMG NMR relaxation dispersion. J. Biomol. NMR *44*, 225–233.

Hendriks, J., and Hellingwerf, K.J. (2009). pH Dependence of the photoactive yellow protein photocycle recovery reaction reveals a new late photocycle intermediate with a deprotonated chromophore. J. Biol. Chem. *284*, 5277–5288.

Hoff, W.D., Devreese, B., Fokkens, R., Nugteren-Roodzant, I.M., Van Beeumen, J., Nibbering, N., and Hellingwerf, K.J. (1996). Chemical reactivity and spectroscopy of

the thiol ester-linked p-coumaric acid chromophore in the photoactive yellow protein from Ectothiorhodospira halophila. Biochemistry *35*, 1274–1281.

Van der Horst, M.A., van Stokkum, I.H., Crielaard, W., and Hellingwerf, K.J. (2001). The role of the N-terminal domain of photoactive yellow protein in the transient partial unfolding during signalling state formation. FEBS Lett. *497*, 26–30.

Imamoto, Y., and Kataoka, M. (2007). Structure and photoreaction of photoactive yellow protein, a structural prototype of the PAS domain superfamily. Photochem. Photobiol. *83*, 40–49.

Imamoto, Y., Mihara, K., Hisatomi, O., Kataoka, M., Tokunaga, F., Bojkova, N., and Yoshihara, K. (1997). Evidence for proton transfer from Glu-46 to the chromophore during the photocycle of photoactive yellow protein. J. Biol. Chem. *272*, 12905–12908.

Imamoto, Y., Harigai, M., and Kataoka, M. (2004). Direct observation of the pH-dependent equilibrium between L-like and M intermediates of photoactive yellow protein. FEBS Lett. *577*, 75–80.

Karplus, S., Snyder, G.H., and Sykes, B.D. (1973). A nuclear magnetic resonance study of bovine pancreatic trypsin inhibitor. Tyrosine titrations and backbone NH groups. Biochemistry *12*, 1323–1329.

Kato-Toma, Y., Iwashita, T., Masuda, K., Oyama, Y., and Ishiguro, M. (2003). pKa measurements from nuclear magnetic resonance of tyrosine-150 in class C beta-lactamase. Biochem. J. *371*, 175–181.

Markley, J.L., Bax, A., Arata, Y., Hilbers, C.W., Kaptein, R., Sykes, B.D., Wright, P.E., and Wüthrich, K. (1998). Recommendations for the presentation of NMR structures of proteins and nucleic acids--IUPAC-IUBMB-IUPAB Inter-Union Task Group on the standardization of data bases of protein and nucleic acid structures determined by NMR spectroscopy. Eur. J. Biochem. FEBS *256*, 1–15.

Mihara, K., Hisatomi, O., Imamoto, Y., Kataoka, M., and Tokunaga, F. (1997). Functional expression and site-directed mutagenesis of photoactive yellow protein. J. Biochem. (Tokyo) *121*, 876–880.

Morishita, T., Harigai, M., Yamazaki, Y., Kamikubo, H., Kataoka, M., and Imamoto, Y. (2007). Array of aromatic amino acid side chains located near the chromophore of photoactive yellow protein. Photochem. Photobiol. *83*, 280–285.

Norton, R.S., and Bradbury, J.H. (1974). Carbon-13 nuclear magnetic resonance study of tyrosine titrations. J. Chem. Soc. Chem. Commun. 870b–871.

Oda, Y., Yamazaki, T., Nagayama, K., Kanaya, S., Kuroda, Y., and Nakamura, H. (1994). Individual ionization constants of all the carboxyl groups in ribonuclease HI from Escherichia coli determined by NMR. Biochemistry (Mosc.) *33*, 5275–5284.

Oktaviani, N.A., Otten, R., Dijkstra, K., Scheek, R.M., Thulin, E., Akke, M., and Mulder, F.A.A. (2011). 100% complete assignment of non-labile (1)H, (13)C, and (15)N signals for calcium-loaded Calbindin D(9k) P43G. Biomol. NMR Assignments *5*, 79–84.

Pellequer, J.L., Wager-Smith, K.A., Kay, S.A., and Getzoff, E.D. (1998). Photoactive yellow protein: a structural prototype for the three-dimensional fold of the PAS domain superfamily. Proc. Natl. Acad. Sci. U. S. A. *95*, 5884–5890.

Prompers, Groenewegen, Hilbers, and Pepermans (1998). Two-Dimensional NMR Experiments for the Assignment of Aromatic Side Chains in 13C-labeled Proteins. J. Magn. Reson. San Diego Calif 1997 *130*, 68–75.

Sigala, P.A., Tsuchida, M.A., and Herschlag, D. (2009). Hydrogen bond dynamics in the active site of photoactive yellow protein. Proc. Natl. Acad. Sci. U. S. A. *106*, 9232–9237.

Sprenger, W.W., Hoff, W.D., Armitage, J.P., and Hellingwerf, K.J. (1993). The eubacterium Ectothiorhodospira halophila is negatively phototactic, with a wavelength dependence that fits the absorption spectrum of the photoactive yellow protein. J. Bacteriol. *175*, 3096–3104.

Takeda, M., Jee, J., Ono, A.M., Terauchi, T., and Kainosho, M. (2009). Hydrogen exchange rate of tyrosine hydroxyl groups in proteins as studied by the deuterium isotope effect on C(zeta) chemical shifts. J. Am. Chem. Soc. *131*, 18556–18562.

Ugurbil, K., and Bersohn, R. (1977). Tyrosine emission in the tryptophanless azurin from Pseudomonas fluorescens. Biochemistry *16*, 895–901.

Ujj, L., Devanathan, S., Meyer, T.E., Cusanovich, M.A., Tollin, G., and Atkinson, G.H. (1998). New photocycle intermediates in the photoactive yellow protein from Ectothiorhodospira halophila: picosecond transient absorption spectroscopy. Biophys. J. *75*, 406–412.

Wilbur, D.J., and Allerhand, A. (1976). Titration behavior of individual tyrosine residues of myoglobins from sperm whale, horse, and red kangaroo. J. Biol. Chem. *251*, 5187–5194.

Xie, A., Hoff, W.D., Kroon, A.R., and Hellingwerf, K.J. (1996). Glu46 donates a proton to the 4-hydroxycinnamate anion chromophore during the photocycle of photoactive yellow protein. Biochemistry *35*, 14671–14678.

Yamaguchi, S., Kamikubo, H., Kurihara, K., Kuroki, R., Niimura, N., Shimizu, N., Yamazaki, Y., and Kataoka, M. (2009). Low-barrier hydrogen bond in photoactive yellow protein. Proc. Natl. Acad. Sci. U. S. A. *106*, 440–444.